Supplementary Document

Karthik Yerrapragada, Haocheng Yang, Wonhyeok Lee, Melih Eriten

1 Pre-stressed thick plate model

To compare the experimental frequency behaviour (Figure 2 of the main manuscript) to predictions of thick plate model, we use equations of motion governing axisymmetric transverse linear vibrations of a pre-stressed thick circular plate from [1]. The solutions of those equations are used to identify the in-plane stress and young's modulus of the gel disk as a function of water loss. The dimensional form of the equations of motion are

$$Gh_f\kappa\left(\frac{\partial^2 w}{\partial r^2}+\frac{1}{r}\frac{\partial w}{\partial r}+\frac{\partial \psi}{\partial r}+\frac{\psi}{r}\right)+N_0\frac{\partial^2 w}{\partial r^2}+\frac{N_0}{r}\frac{\partial w}{\partial r}=\rho h_f\ddot{w} \tag{S.1}$$

$$(D+M_0)\left(\frac{\partial^2 \psi}{\partial r^2}+\frac{1}{r}\frac{\partial \psi}{\partial r}-\frac{\psi}{r^2}\right)-Gh_f\kappa\left(\frac{\partial w}{\partial r}+\psi\right)=\frac{\rho h_f^3}{12}\ddot{\psi} \tag{S.2}$$

where ($\dot{}$) refers to time derivative, r is the radial coordinate, G is the shear modulus, h_f is the thickness of the plate at a given water loss state and κ is the shear correction factor. $w(r,t)$ is with respect to the center of the mid-plane of the undeformed plate. Flexural rigidity of the plate is defined as $D = Eh_f^3/\left[12\left(1-\nu^2\right)\right]$, where E is the Young's modulus and ν is the Poisson's ratio of the gelatine sample. In-plane inertial forces are expected to be small during the transverse vibrations and only involve in-plane motion. Therefore, the equations of motion governing the axisymmetric transverse displacement $w(r,t)$ and rotation $\psi(r,t)$ of the cross section suffice for our study. With uniformly distributed initial stress σ_0 along the radial and circumferential directions, $N_0 = \sigma_0 h_f$ and $M_0 = \sigma_0 h_f^3/12$.

At a given water loss state, E, ρ and the radius of the plate R are constant and thus can provide relevant length and time scales for the dependent and

independent variables in Equation S.1 and S.2. Defining those scales as $\xi = \frac{r}{R}$ and $\tau = \omega_0 t$ with $\omega_0 = \frac{1}{R}\sqrt{\frac{E}{\rho}}$, one can convert the equations of motion into a non-dimensional form

$$\frac{\kappa}{2(1+\nu)}\left(\frac{\partial^2 W}{\partial \xi^2} + \frac{1}{\xi}\frac{\partial W}{\partial \xi} + \frac{\partial \psi}{\partial \xi} + \frac{\psi}{\xi}\right) + \beta\left(\frac{\partial^2 W}{\partial \xi^2} + \frac{1}{\xi}\frac{\partial W}{\partial \xi}\right) = W'' \quad \text{(S.3)}$$

$$\left(\frac{1}{1-\nu^2} + \beta\right)\left(\frac{\partial^2 \psi}{\partial \xi^2} + \frac{1}{\xi}\frac{\partial \psi}{\partial \xi} - \frac{\psi}{\xi^2}\right) - \frac{6\kappa\alpha^2}{1+\nu}\left(\frac{\partial W}{\partial \xi} + \psi\right) = \psi'' \quad \text{(S.4)}$$

where the $W(\xi, \tau)$ are the transverse vibrations normalized to the radius of the disk and ($'$) refers to derivative with respect to normalized time τ. Note that isotropic linear elastic response with $G = E/\left[2(1+\nu)\right]$ is assumed in simplifications leading to Equations S.3 and S.4 with two key parameters $\alpha = \frac{R}{h_f}$ and $\beta = \frac{\sigma_0}{E}$.

As mentioned in the main manuscript, the increase of in-plane stresses would change the plate to membrane where tension dominates the bending rigidity. This is reflected in Equation S.3 as a large β will make terms in the second parentheses more significant and they are similar to the governing equations of vibrations of circular membrane. Another additional point to be noted, the effect of any variation of Young's modulus along the gel thickness was found to have minimal (second order change) in the frequencies. The effect of varying Young's modulus along the thickness was studied using Finite Element Analysis. The Young's modulus was assumed to increase from the mid plane to the top and bottom of the disk. The mathematical form (close to quadratic) was obtained from the solution of diffusion equation based on water loss along thickness. With the identified stress σ_0 and Young's modulus E values at a given water loss level of a disk, changing Young's modulus from the uniform value E to a thickness dependent form did not significantly change the frequency ratio and values (second order change). Thus, we conclude that any Young's modulus gradient along the thickness has smaller order effect compared to in-plane stress effect. Equations S.3 and S.4 are given as Equations 1 and 2 in the Section 2.3 of the main manuscript. The boundary and symmetry conditions for the disk clamped at $\xi = 1$ are

$$\begin{aligned} W(1,\tau) &= \psi(1,\tau) = 0 \\ \frac{\partial W}{\partial \xi}(0,\tau) &= \psi(0,\tau) = 0 \end{aligned} \quad \text{(S.5)}$$

The Galerkin's method is then used to obtain the natural frequencies ω of the transverse vibrations. First, approximate synchronous solutions of Equations S.3 and S.4 satisfying the boundary conditions listed above are assumed

$$\begin{aligned} W(\xi,\tau) &= \left[AW_1(\xi) + BW_2(\xi) + CW_3(\xi)\right] e^{i\lambda\tau} \\ \psi(\xi,\tau) &= \left[H\psi_1(\xi) + I\psi_2(\xi) + J\psi_3(\xi)\right] e^{i\lambda\tau} \end{aligned} \tag{S.6}$$

where

$$W_i(\xi) = \left(1-\xi^2\right)^2 \xi^{2i-2},\ \psi_i(\xi) = -\frac{dW_i}{d\xi},\ \lambda = \frac{\omega}{\omega_0} \tag{S.7}$$

and A, B, C, H, I and J are the weights of the spatial functions approximating the mode shapes of the transverse vibrations of a thin circular plate. Re-defining the equations of motion as operators $L_W(W,\psi)$ and $L_\psi(W,\psi)$

$$\begin{aligned} L_W(W,\psi) =& \frac{\kappa}{2(1+\nu)}\left(\frac{\partial^2 W}{\partial\xi^2} + \frac{1}{\xi}\frac{\partial W}{\partial\xi} + \frac{\partial\psi}{\partial\xi} + \frac{\psi}{\xi}\right) \\ &+ \beta\left(\frac{\partial^2 W}{\partial\xi^2} + \frac{1}{\xi}\frac{\partial W}{\partial\xi}\right) - W'' \end{aligned} \tag{S.8}$$

$$\begin{aligned} L_\psi(W,\psi) =& \left(\frac{1}{1-\nu^2} + \beta\right)\left(\frac{\partial^2\psi}{\partial\xi^2} + \frac{1}{\xi}\frac{\partial\psi}{\partial\xi} - \frac{\psi}{\xi^2}\right) \\ &- \frac{6\kappa\alpha^2}{1+\nu}\left(\frac{\partial W}{\partial\xi} + \psi\right) - \psi'' \end{aligned} \tag{S.9}$$

and taking inner products with W_i and ψ_i (averaging over the disk radius)

$$\begin{aligned} \langle L_W(W,\psi), W_i\rangle &= \int_0^1 L_W(W,\psi) W_i \xi d\xi = 0 \\ \langle L_\psi(W,\psi), \psi_i\rangle &= \int_0^1 L_\psi(W,\psi)\psi_i \xi d\xi = 0 \end{aligned} \tag{S.10}$$

yields six linear equations with the unknown weights, A, B, C, H, I and J. These equations can be written in matrix form as

$$\mathbf{Qx} = \mathbf{0} \tag{S.11}$$

where $\mathbf{Q}$ is a 6×6 matrix whose elements depend on α, β, λ, ν and κ, and $\mathbf{x} = [A, B, C, H, I, J]^T$. For nontrivial solutions of Equation S.11, $|\mathbf{Q}| = 0$, which can be solved for six positive λ values for a given set of α, β, ν and κ parameters. The two smallest λ's, λ_1 and λ_2, correspond to the natural frequencies $\omega_1 = 2\pi f_1$ and $\omega_2 = 2\pi f_2$ of the first two axisymmetric modes. Note that the results in the main manuscript (e.g., Fig.2) are given in terms of f_1 and f_2.

2 Theoretical and experimental mode shapes

To obtain theoretical mode shapes, the weights $\mathbf{x}$ in Equation S.6 should be obtained for each mode; i.e., substitute λ_i into $\mathbf{Q}$ in Equation S.11, set one of the weights arbitrarily to 1, say $A = 1$ and solve the other unknown weights. For experimental mode shapes, we first create a geometry mesh on the gel disks. The mesh consiste of 140 sensing locations, which can successfully resolve the first two axisymmetric modes. The gel disks are then vibrated harmonically at resonance frequencies and response is recorded via scanning laser vibrometry (PSV400, Polytec Inc.). The mode shapes are directly constructed via the Polytec software.

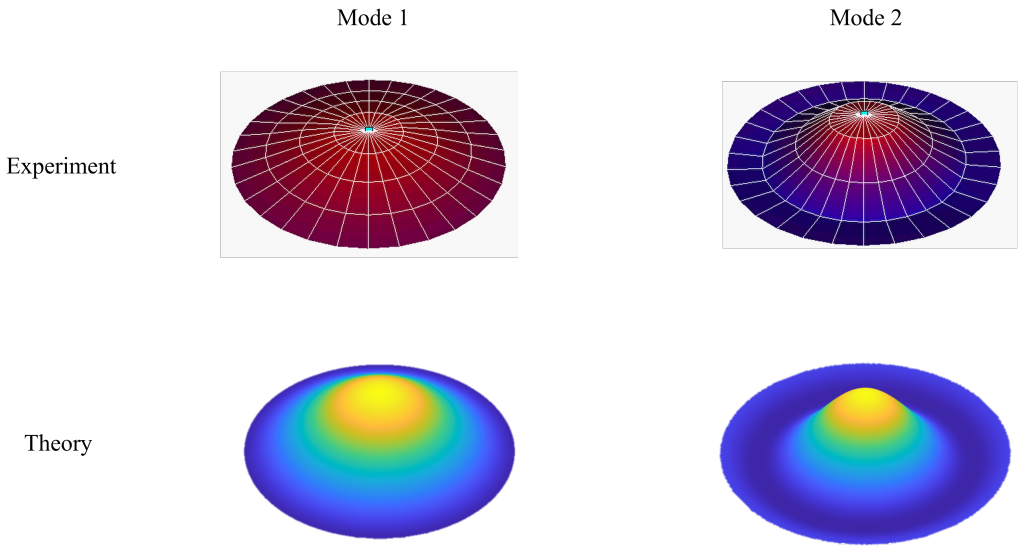

Figure S1: Comparison of theoretical and experimental mode shapes for the wet case.

Figs. S1 and S2 show the comparison between the theoretical and experimental mode shapes at wet and 80 wt.% dry cases, respectively for the first two axisymmetric modes. Mode shapes match reasonably well between theory and experiments. Experimental mode shapes are also illustrated as insets in Fig.2 of the article.

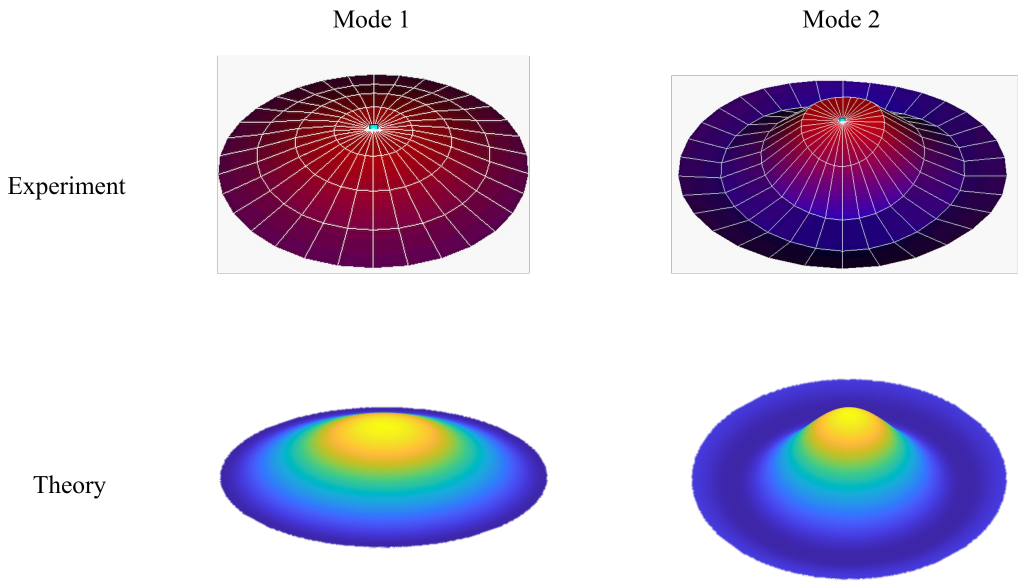

Figure S2: Comparison of theoretical and experimental mode shapes for the 80 wt.% dry case.

3 Evolution of sample thickness with dehydration

To independently gauge the effect of water loss on the sample thickness, we prepared three additional disk samples using the same protocol described in Section 2.1 of the main manuscript. The radius (15 mm) and initial thickness ($\sim$ 4 mm) of the samples are similar to the ones used in the vibration testing. The samples are then subjected to dehydration as described in the main manuscript. At regular intervals, we monitor the weight and thickness of the disks. We use a digital thickness gauge (BNISE) for thickness measurements. The thickness varies slightly from the center to a thin region around the clamped boundary, and attains the maximum value at the boundary (the initial thickness, h_0). We report the thickness at the center of the disk h_f in Figure S3. Thickness decreases linearly up to 60 wt.% water losses. The obtained information is used in Section 3.2 of the main manuscript to study the effect of in-plane stress and thickness reduction on the frequency ratio of the two vibration modes of the disk.

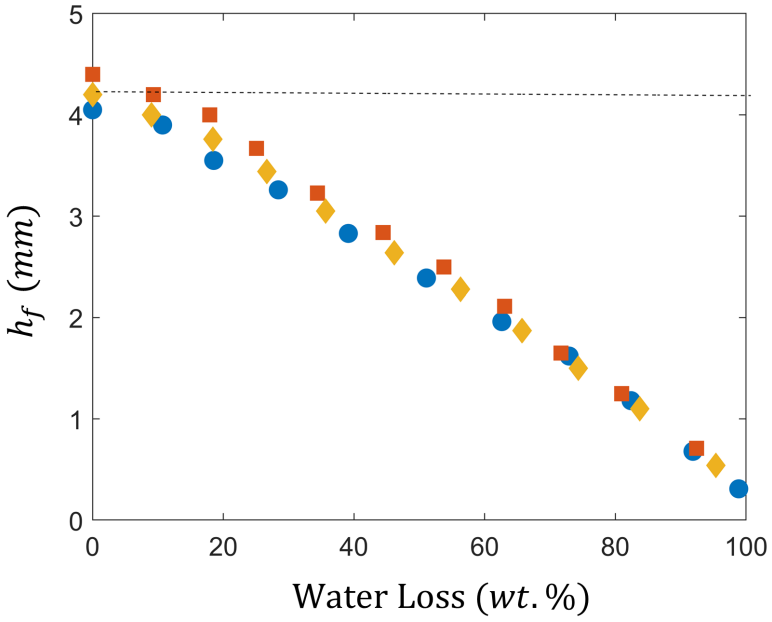

Figure S3: Evolution of disk thickness with water loss

4 Modulus characterization with and without internal stress

Figure 3B of the main manuscript shows the Young's modulus characterization from the methodology developed in this paper that contains the effect of internal stress. The mean modulus of the six samples is plotted in Figure S4 using red markers. In addition, the modulus characterized without internal stress is plotted using blue markers. The characterized moduli diverge as the material continues to dehydrate. The moduli characterized without internal stress reach 2 MPa at the largest water loss. Those values are beyond the range of moduli reported for gelatin. The characterization with internal stress deliver moduli close to 400 kPa, still within reasonable range reported for high concentration gels. This comparison clearly demonstrates the importance of internal stress formulation in mechanical characterization of constrained gels.

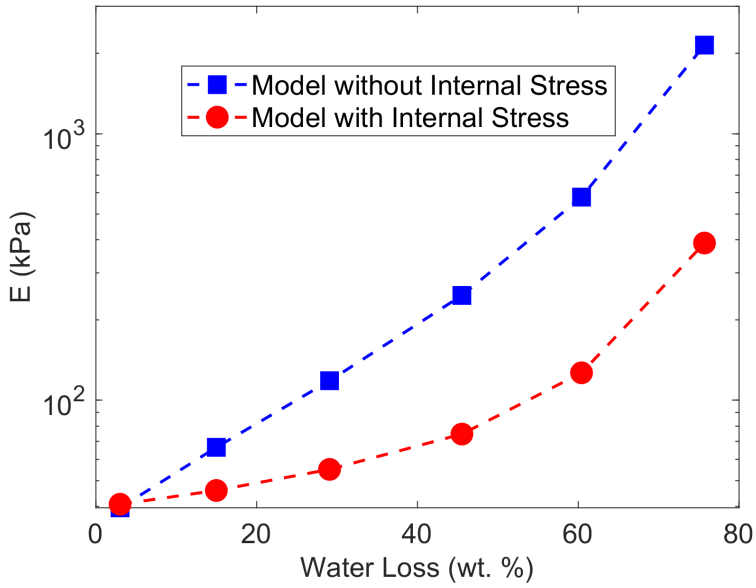

Figure S4: Young's modulus characterization from models with and without consideration of internal stress

5 Indentation-based modulus characterization

We have conducted calibration by displacement-controlled indentation on the gelatin samples at wet states. In those experiments, we measured both load P and contact radius a, and used standard JKR based theory [2] to fit the contact modulus E^* and work of adhesion $\Delta\gamma$ from the experimental data:

$$a^3 = \frac{3R}{4E^*}\left(P + 3\pi\Delta\gamma R + \sqrt{6\pi\Delta\gamma RP + (3\pi\Delta\gamma R)^2}\right) \tag{S.12}$$

The Young's modulus of the sample E was estimated from the contact modulus using $E^* = E/(1-\nu^2)$ and Poisson's ratio $\nu = 0.48$. The gelatin samples tested were cylinders with 85 mm diameter and 13 mm thickness. The thickness selected for the samples is about 3 times higher than the vibration samples. The larger thickness ensured that boundary effects during indentation were negligible. The indenter was a sphere made of glass (assumed $E = 65$ GPa, $\nu = 0.3$) with a radius $R = 51.68$ mm (rigid indenter compared to the sample compliance). The sample was loaded slowly at 0.1 mm/s. The average Young's modulus obtained from 5 indentation experiments was 33 kPa,

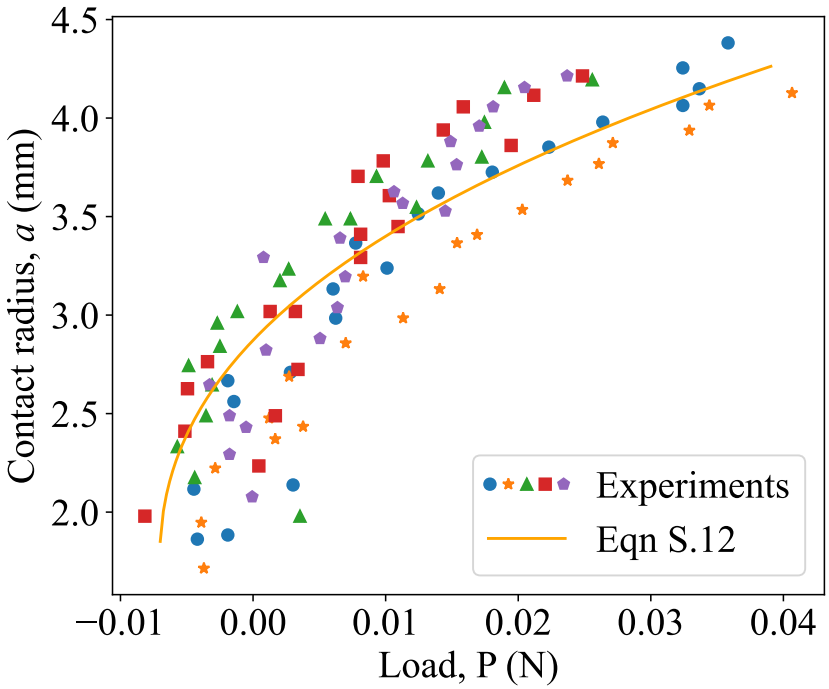

Figure S5: Contact radius vs load obtained from five indentations and the JKR theory given in Equation S.12 fit to the average of the experiments.

which is close to the average modulus obtained from vibration experiments approximately 40 kPa. See Figure S5 for the indentation fit.

About 17.5% difference in moduli could be attributed to the slow indentation rates compared to the modal frequencies (40 Hz for the smallest modal frequency that we measured). During the indentation tests, we were measuring the relaxed modulus. In gels, relaxations could be due to reconfiguration of solid network (viscoelasticity) and diffusion driven by pressure gradients (poroelasticity). At macroscopic length scales applicable to both vibration and indentation tests, poroleastic relaxations could be neglected and thus most of the reduction in moduli can be primarily attributed to viscoelastic relaxations. In addition, indentation tests are sensitive to local variations in water-solid content in the samples, but vibration-based moduli are averaged through the whole volume active in both modes of vibration. Near-surface indents are known to produce slightly lower moduli than the bulk in gels; due to functionally-gradient microstructure (e.g., polyacrylamide tested via local methods as AFM [3] and indentation [4] versus macroscopic uniaxial

compression [5]). So, some portion of the deviations can be attributed to those local effects in indentation tests.

References

[1] Lien-Wen Chen and Ji-Liang Doong. Vibrations of an initially stressed transversely isotropic circular thick plate. *International journal of mechanical sciences*, 26(4):253–263, 1984.

[2] Kenneth Langstreth Johnson, Kevin Kendall, and aAD Roberts. Surface energy and the contact of elastic solids. *Proceedings of the royal society of London. A. mathematical and physical sciences*, 324(1558):301–313, 1971.

[3] Ramesh Subramani, Alicia Izquierdo-Alvarez, Pinaki Bhattacharya, Mathieu Meerts, Paula Moldenaers, Herman Ramon, and Hans Van Oosterwyck. The influence of swelling on elastic properties of polyacrylamide hydrogels. *Frontiers in Materials*, 7:212, 2020.

[4] Yuki A Meier, Kaihuan Zhang, Nicholas D Spencer, and Rok Simic. Linking friction and surface properties of hydrogels molded against materials of different surface energies. *Langmuir*, 35(48):15805–15812, 2019.

[5] Edvani C Muniz and Georges Geuskens. Compressive elastic modulus of polyacrylamide hydrogels and semi-ipns with poly (n-isopropylacrylamide). *Macromolecules*, 34(13):4480–4484, 2001.